Fire Safety Journal 153 (2025) 104381

Contents lists available at ScienceDirect

Fire Safety Journal

journal homepage: www.elsevier.com/locate/firesaf

Toxic gas and particle emissions from the pyrolysis of spacecraft materials

Bjoern Bingham [a,b], Salix Bair [a,b], Matthew Claassen [a,b], Marit E. Meyer [c,1], Claire Fortenberry [c], W. Patrick Arnott [b], John G. Watson [a], Judith C. Chow [a], Xiaoliang Wang [a,b,*]

[a] Desert Research Institute, 2215 Raggio Pkwy, Reno, NV, 89512, USA
[b] University of Nevada, Reno, 1664 N. Virginia Street, Reno, NV, 89557, USA
[c] NASA Glenn Research Center, 21000 Brookpark Road, Cleveland, OH, 44135, USA

ARTICLE INFO

Keywords:
Spacecraft
$PM_{2.5}$
HF
HCN
Particle size distribution
Emission factor
Particle charge distribution
PTFE
Kapton
Fire safety

ABSTRACT

Fire is an imminent risk in space activities. Toxic gas and particle emissions can quickly reach dangerous levels in sealed environments. To improve smoke detection, protection, and post-fire cleanup, understanding the emissions from the pyrolysis of spacecraft-relevant materials is crucial. This study investigated the pyrolysis of four common spacecraft materials, including Kapton, polytetrafluoroethylene (PTFE), Teflon/Kapton/Teflon (TKT) wire insulation, and Velcro™, to identify, evaluate, and quantify their gaseous and particulate emissions. Kapton emitted high levels of carbon monoxide and hydrogen cyanide, PTFE and TKT emitted multiple toxic fluorine-based gases including carbonyl fluoride and hydrogen fluoride, while Velcro™ had the highest $PM_{2.5}$ emission factor. Most particles were in the submicron size range, with mode diameter peaked in the 100–200 nm range. The particles were nearly electrically neutral, carrying less than 0.15 net elementary charges per particle. Organic compounds predominated in the particle compositions.

1. Introduction

Fires in space activities pose an immediate danger to astronauts, equipment, and mission viability. As mission durations increase, the chances of fire are likely to increase [1,2]. Fire risks in the sealed spacecraft environment are greater than in most terrestrial locations because toxic gases and particles can quickly reach dangerous levels. Limited methods exist to suppress these fires, ventilate smoke, and evacuate occupants. Characterizing emissions from burning spacecraft materials is crucial for designing smoke detectors, respirators, fire extinguishers, post-fire cleanup strategies, and understanding long-term health impacts.

A growing fire must be detected as early as possible to prevent escalation into a more severe scenario. In the event of a survivable fire [3], mitigation measures should be implemented to reduce toxic combustion and pyrolysis byproducts. However, traditional spacecraft fire detection methods, which are based solely on detecting smoke particles (e.g., for space shuttles and the International Space Station [ISS]), face challenges in the novel spacecraft environment. On Earth, smoke rises and accumulates at the ceiling due to buoyancy, enabling early detection at the ceiling. In microgravity, this natural concentration mechanism does not occur, and particle transport is dominated by turbulent mixing driven by the Environmental Control and Life Support System (ECLSS). Urban et al. [4] show that the rapid particle filtration rates typical of the ISS ECLSS may outpace smoke emission rates in the early stage of a fire, increasing the likelihood that the fire will go undetected. These results suggest that adding gas-phase detection targets, such as carbon monoxide (CO), could enable faster and more reliable fire detection than particle detection alone, since gases are not subject to this rapid filtration [4]. Furthermore, studies of spacecraft smoke demonstrate that current smoke detector technologies vary in reliability depending on the properties of smoke particles. Meyer et al. [2] report that the ISS fire detector did not reliably alarm for PTFE and Kapton smoke, two materials commonly found on the ISS, especially in electrical wire insulation, where early fires might start. Together, these results suggest that no single detection method can effectively detect all spacecraft fire scenarios, and a combined detection approach targeting both particles and gases could improve early fire detection.

Characterizing toxic gases from spacecraft material pyrolysis is essential to assess the risk and potential outcomes of spacecraft fires [5]. This underscores the need for improvements in *in situ* trace contaminant analysis, especially as longer missions farther from Earth (e.g., to the

* Corresponding author. Desert Research Institute, 2215 Raggio Pkwy, Reno, NV, 89512, USA.
E-mail address: Xiaoliang.Wang@dri.edu (X. Wang).
[1] Present address: Northrop Grumman, 16055 Space Center Blvd, Houston, TX 77062, USA.

https://doi.org/10.1016/j.firesaf.2025.104381
Received 18 December 2024; Received in revised form 19 March 2025; Accepted 20 March 2025
Available online 21 March 2025

Moon) are planned. While major atmospheric gases on the ISS (i.e., nitrogen [N_2], oxygen [O_2], carbon dioxide [CO_2], methane [CH_4], hydrogen [H_2], and water vapor [H_2O]) are measured by the mass-spectrometer-based Major Constituent Analyzer (MCA) [6], trace contaminant concentrations are typically characterized through bottle collections and ground-based analysis. Motivated by the need to monitor and respond to atmospheric toxicants without ground support, NASA has prioritized the development of *in situ* trace gas analyzers [7,8], including two laser absorption-based gas sensors developed specifically for monitoring spacecraft fire byproducts: the Anomaly Gas Analyzer (AGA; Vista Photonics) and the Combustion Products Monitor (CPM; Jet Propulsion Laboratory [JPL]). The most recent version of the AGA monitors nine gases (CO, CO_2, hydrogen cyanide [HCN], hydrogen fluoride [HF], hydrochloric acid [HCl], O_2, H_2O, ammonia [NH_3], and hydrazine [N_2H_4]), while the CPM monitors O_2, CO, CO_2, HCN, HF, and HCl. O_2 is essential for life, while H_2O is important for comfort and hydration. CO, CO_2, HCN, HF, and HCl are toxic fire byproducts, whereas NH_3 and N_2H_2 may indicate a leak from temperature control loop or propellant system. Both the AGA and the CPM have been flight-demonstrated with microgravity fires during the Spacecraft Fire Safety (Saffire) suite of experiments [9,10], and the AGA has also been flight-tested aboard the ISS [11]. Prior to flight, the AGA and CPM were ground-tested alongside *in situ* reference measurements for targeted analytes. *Ex-situ* reference measurements, including gas chromatography, mass spectrometry, and ion chromatography, were also obtained during this test campaign to analyze the fire signatures of various spacecraft materials. However, further work is needed to investigate the evolution of gases throughout an oxidative pyrolysis event [12]. Fourier-transform infrared spectroscopy (FTIR) gas analyzers are ideal tools for identifying and quantifying gases emitted from fires in real time [13], especially when the full range of gases produced during a fire or pyrolysis event is not yet understood.

Particle size and charge distributions influence smoke detection, penetration through respirators, and deposition in the human respiratory tract. Several past studies used instruments that were too slow (1–2 min per scan) to accurately capture transient size changes [14–16]. Fast-size distribution measurement instruments, such as the Electrical Low-Pressure Impactor (ELPI; Dekati Ltd) [17–20], can measure size distributions at 0.1-s intervals. The ELPI can also measure the natural charge distributions carried by particles [21]. These features make the ELPI an attractive choice for measuring the size and charge distribution of smoke particles.

The goal of this study is to better understand the gas and particulate emissions from the pyrolysis of modern spacecraft materials. The specific objectives are to: 1) characterize toxic gas emissions from spacecraft material pyrolysis; 2) measure particle size and charge distributions as well as chemical compositions; and 3) determine emission factors for gases and particles.

2. Materials and methods

2.1. Sample materials

This study measured pyrolysis emissions from four common spacecraft materials (pictured in Fig. S1), including Kapton, PTFE (polytetrafluoroethylene; Teflon), Teflon/Kapton/Teflon (TKT) wire insulation (Thermax M66759/86-20-9), and Velcro™. Kapton is a Poly (4,4′-oxydiphenylene-pyromellitimide) film with a chemical formula of $C_{22}H_{10}N_2O_5$ (Fig. S2a). It is typically used in electronics, spacesuits, and spacecraft shielding for electrical and thermal insulation [22]. It is thermally stable over a wide temperature range from −269 to 400 °C. Kapton is self-extinguishing with the highest UL-94 flammability rating of V-0. PTFE is a synthetic fluoropolymer of tetrafluoroethylene with a chemical formula of $(CF_2\text{-}CF_2)_n$ (Fig. S2b). PTFE is commonly used for wire insulation, water storage bladders, sampling bags, suits, and cargo liners and has a melting point of ~327 °C. TKT wire insulation (Fig. S3) is widely used in aeronautics and space industries due to its improved thermal/fire-resistant properties as compared to PVC or Kapton insulation with current varieties performing up to 260 °C [23]. Adhesive-backed Velcro™ circles made out of Nylon, also called Velcoins™, are commonly used to secure items during transport or as fasteners under low gravity environments. Velcro™ is the most flammable of the four test materials, so wall-mounted quantities are limited on the ISS. The flaming behavior of nylon Velcro™ was observed by Olson and Sotos [24] in low gravity. All these materials experience oxidative pyrolysis and emit smoke when exposed to overheating such as in an electrical short circuit.

To allow test materials to be inserted into the NASA White Sands Smoke Generator (WSSG; Fig. S4), the Kapton film was cut into ~8 mm × 8 mm squares or smaller, as shown in Fig. S1a. PTFE came in the form of a 5 mm diameter cord that was cut into 1–3 mm lengths (Fig. S1b). The TKT (Fig. S1c) insulation consists of a Teflon-coated exterior bonded to a Teflon sleeve around a layer of Kapton, with the innermost sleeve being Teflon as shown in Fig. S3. The insulation was stripped from 20 American wire gauge (AWG) aerospace-grade wire, cut open to expose the Kapton interior, and then cut into 5 mm or shorter pieces for heater insertion. The Velcro™ (Fig. S1d) was procured as 1.3 cm-diameter Velcoins™, circular pieces with adhesive backing.

The carbon (C), hydrogen (H), nitrogen (N), and sulfur (S) elemental compositions of the sample materials and the ashes after pyrolysis were measured using an Elemental Analyzer (Model Flash EA1112, Thermo Scientific), and the data are summarized in Tables S1 and S2. Average sample sizes and percent of original mass for the ash are listed in Tables S1 and S2 as well.

2.2. Oxidative pyrolysis experiments

The WSSG (Fig. S4) was used to pyrolyze sample materials and generate smoke under controlled conditions. This device was developed by NASA to establish a standard smoke generation method for characterizing combustion and pyrolysis emissions from spacecraft-relevant materials [12]. The test material was wrapped in a mica sheet and placed inside the quartz tube heater with an inner diameter of 2.54 cm. The heating temperature can be set between room temperature and 650 °C at defined ramping rates. The smoke was carried out of the heater at 3 L min^{-1} driven by a diaphragm pump. As illustrated in Fig. S5, this study used a 30-min ramp from room temperature to 640 °C to evaluate pollutant emissions at different temperatures. The temperature was held at 640 °C for 30 min. After that, the setpoint temperature was reduced to 22 °C which required ~10 min to return to room temperature.

As shown in Fig. 1, the WSSG was placed in the middle of the combustion chamber and the vented gases and particles were measured by a suite of analyzers described in previous publications [16,25,26]. Up to 50 gases including volatile organic compounds (VOCs) were measured by an FTIR multi-gas analyzer (Model GT5000 Terra, Gasmet Technologies), which sampled close to the WSSG exhaust port, through a ~1 m length of PTFE tubing to reduce transport losses of sticky gases. FTIR has been widely used to measure combustion byproducts, including HF. However, actual HF concentrations may be higher than the measured values due to its high solubility in water, which can lead to condensation on the walls [27]. CO_2, CO, oxides of nitrogen (NO, NO_2, and NO_x), and sulfur dioxide (SO_2) were sampled at the same location as the FTIR and measured by a suite of gas analyzers (Table S3). Particle concentrations were sampled from the smoke stack via conductive tubing to minimize electrostatic losses. The ELPI measured particle size distributions from 6 nm to 10 μm in 100 channels every second from a diluted sample line to prevent impactor overloading [18,28]. The dilution ratio was determined by the particulate matter (PM) concentration ratios measured by two DustTrak DRX (Model 8534, TSI Inc.) before and after dilution [25,29]. The ELPI also measured particle net charge distributions in separate tests by alternatively turning the charger on and off [30]. FTIR and ELPI were used by Ngohang et al. [31] to characterize gases and particle size

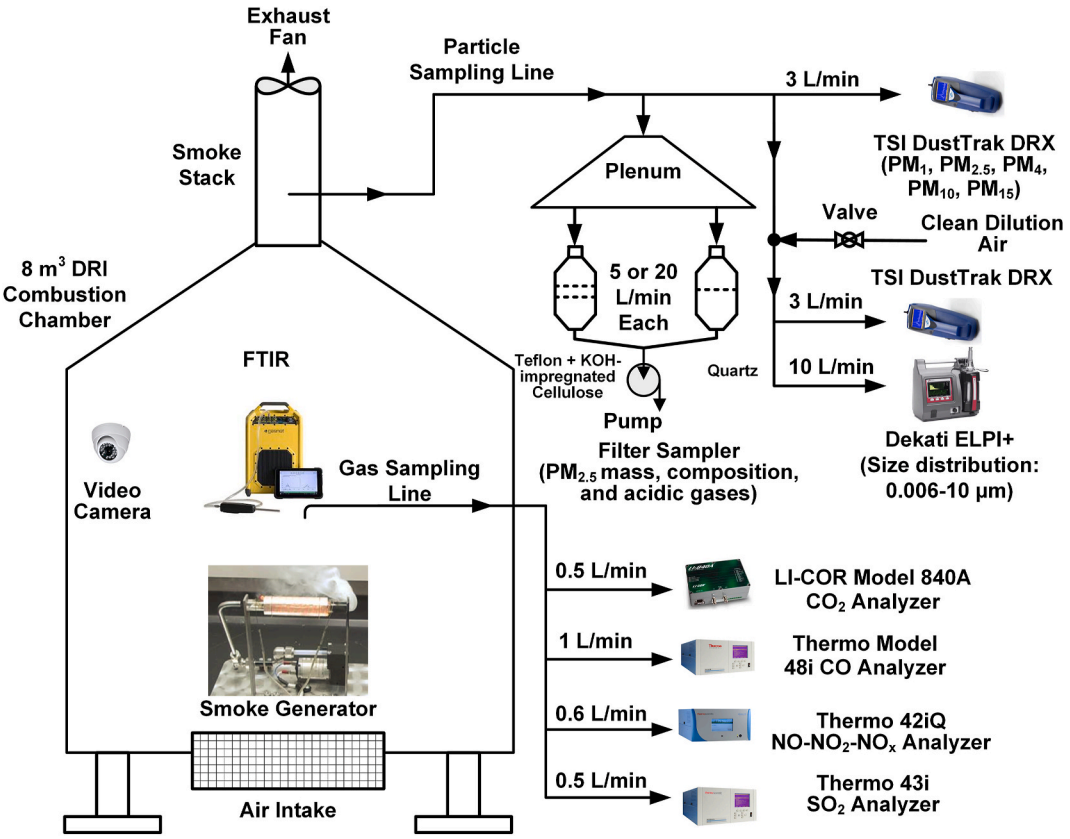

Fig. 1. Experimental setup for pyrolysis experiments.

distributions emitted from ethylene vinyl acetate fires.

$PM_{2.5}$ was collected on two parallel filter channels for chemical composition analyses [26,32]. Channel 1 contained a Teflon membrane filter, which was analyzed for $PM_{2.5}$ mass by gravimetry and 51 elements (from Na to U) by an X-ray fluorescence (XRF) analyzer. Channel 2 contained a quartz-fiber filter, half of which was analyzed for ten water-soluble ions, including ammonium (NH_4^+), sodium (Na^+), magnesium (Mg^{2+}), potassium (K^+), calcium (Ca^{2+}), fluoride (F^-), chloride (Cl^-), nitrite (NO_2^-), nitrate (NO_3^-), and sulfate (SO_4^{2-}) by ion chromatography (IC). A 0.5 cm^2 punch of the quartz-fiber filter was analyzed for organic and elemental carbon (OC and EC) as well as eight thermal fractions (i.e., OC1 – OC4, pyrolyzed carbon [OP], EC1 – EC3) following the IMPROVE_A thermal optical analysis protocol [33].

The measured chemical compositions were grouped into five major categories to calculate reconstructed mass: organic matter (OM = OC × f_{OC}), EC, ions, geological materials (2.2 × Al + 2.49 × Si + 1.63 × Ca +2.42 × Fe + 1.94 × Ti), and other measured species without double counting [34]. The f_{OC} multiplier, which accounts for unmeasured species such as hydrogen and oxygen, was calculated as the difference between gravimetric mass and the sum of species other than OC divided by OC. The average f_{OC} values were 1.2 for Kapton and Velcro™ and 2.86 for PTFE and TKT. The f_{OC} for PTFE and TKT is greater than typical values (1.2–2.6), probably caused by unmeasured chemical species such as fluorine in fluorinated carbon-based compounds.

2.3. Emission factor calculation

Fuel-based emission factors (EF, in g/kg fuel) were calculated based on the carbon mass balance technique [16,35,36].

$$EF_i = \left(CMF_{fuel} - \frac{m_{ash}}{m_{fuel}} CMF_{ash}\right) \frac{C_i}{C_{CO_2}\left(\frac{M_c}{M_{CO_2}}\right) + C_{CO}\left(\frac{M_c}{M_{CO}}\right) + C_{CH_4}\left(\frac{M_c}{M_{CH_4}}\right) + \sum_j C_{VOC_j}\left(\frac{n_j \times M_c}{M_{VOC_j}}\right) + C_{PM}} \times 10^3 \quad (1)$$

where CMF_{fuel} and CMF_{ash} are the carbon mass fraction of the fuel and ash in g carbon per g of fuel material (Table S1) and ash (Table S2), respectively. m_{fuel} and m_{ash} are the mass of fuel and ash in g, respectively. C_i is the background-subtracted plume concentration of pollutant i in g/m^3 (including species containing and not containing carbon); and C_{CO_2}, C_{CO}, C_{CH_4}, and C_{VOC_j} are the concentrations of CO_2, CO, CH_4, and VOC species j above background concentrations in g/m^3, respectively. C_{PM} is the $PM_{2.5}$ total carbon concentration in g/m^3. M_C, M_{CO_2}, M_{CO}, M_{CH4}, and M_{VOC_j} are the atomic or molecular weights of carbon, CO_2, CO, CH_4, and VOC species j in g per mole, respectively. n_j is the number of carbon atoms in VOC species j. The factor of 1000 converts mass from kilograms to grams. This method assumes that the target pollutants are homogeneously mixed with carbon species and proportionally distributed in the plume [36]. Eq. (1) assumes that the carbon mass in emissions other than CO_2, CO, CH_4, VOCs measured by FTIR, and $PM_{2.5}$ is negligible, which is a reasonable assumption for such burns. However, it is recognized that some VOCs are not measured by FTIR, resulting in

slightly overestimated EFs. Since PM was sampled from smoke stack with greater dilution, its concentrations were lower than those measured at the WSSG outlet. Given that C_{PM} accounted for 1 %, 1 %, 3 %, and 10 % of the emitted carbon (denominator of Eq. (1)) for the four fuel materials, using the lower C_{PM} would result in a slight overestimation of gas EFs and an underestimation of particle EFs.

It should be noted that these experiments were run in Reno, Nevada, USA at ~5000 feet (1524 m) of elevation, where the oxygen partial pressure is ~17 % lower than that at sea level. The average ambient temperature of the combustion chamber at the start of experiments was ~25 °C and air pressure was generally ~840 mbar. All concentrations were converted to standard temperature and pressure in emission factor calculations.

The EFs allow the estimation of expected emissions if a fire or overheating event were to occur, based on how much fuel materials were pyrolyzed. This can influence clean-up procedures, safety precautions, ventilation design, and smoke detector design.

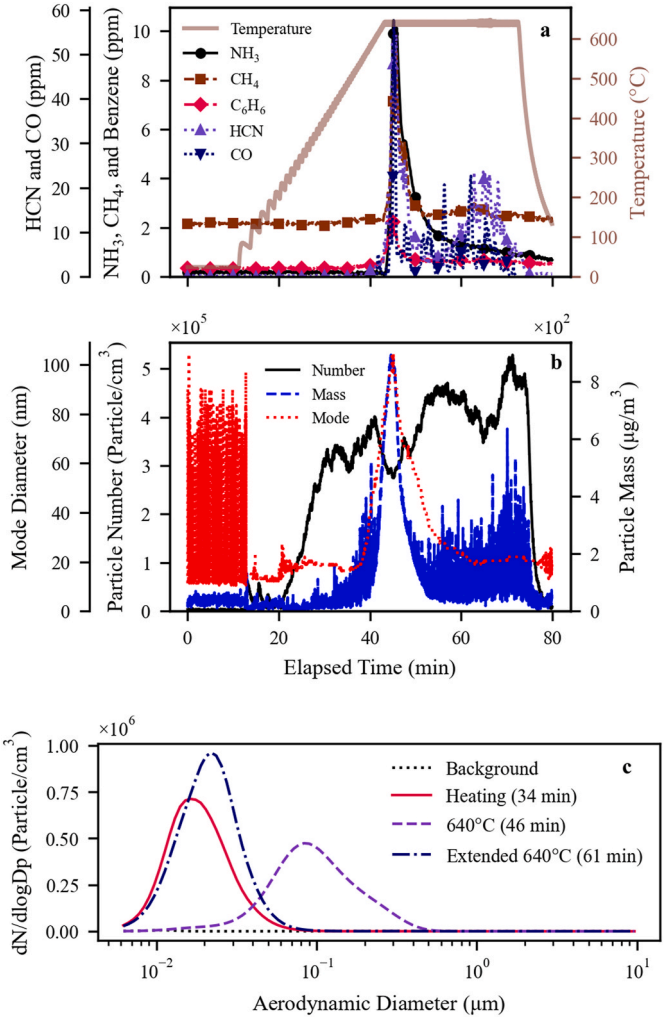

Fig. 2. Results from a Kapton experiment: a) time series gas concentrations at different temperatures for ammonia (NH_3), methane (CH_4), benzene (C_6H_6), hydrogen cyanide (HCN), and carbon monoxide (CO); b) time series of particle number and mass concentrations as well as mode diameters; c) snapshots of particle size distributions at four stages: background, during the heat ramping, when the max setpoint was reached, and the extended heating at 640 °C.

3. Results & discussion

3.1. Emission characteristics

3.1.1. Kapton

Kapton pyrolysis generated several gases identified by the FTIR with high signal-to-noise ratios. Fig. 2a shows that HCN levels reached as high as 55 ppm, exceeding the Immediately Dangerous to Life or Health Concentration (IDLH) limit of 50 ppm by the National Institute for Occupational Safety and Health [37]. HCN is approximately 25 times more toxic than CO [5]. Based on NASA's Spacecraft Maximum Allowable Concentrations (SMACs), any concentration over 8 ppm has notable impacts on the central nervous system after just 1 h of exposure to HCN [38]. However, it should be noted that the gases were measured close to the WSSG outlet. Dilution by ventilation air will likely lower the concentrations in a real-world spacecraft. In addition to this major peak at ~45 min at 640 °C, a secondary peak occurred at 55–70 min with lower concentrations, likely due to further decomposition of Kapton films. Ortelli et al. [39] observed that Kapton thermally decomposes in distinct steps: first, the imide ring without elimination of the carbonyl groups, followed by the decomposition of the aromatic and carbonyl groups. CO emissions were sporadic, with peak concentrations reaching ~60 ppm. NH_3, and CH_4 were also emitted from Kapton pyrolysis, coinciding with the main HCN peak. Benzene (C_6H_6) emissions are unique to Kapton and TKT wire insulation emissions.

As shown in Fig. 2b and Fig. S6, particle number concentrations fluctuated when the heater started ramping (12–18 min; <200 °C), similar to previous observations in a tube furnace experiment [40]. The concentration increased after the temperature exceeded ~200 °C (~20 min). The particle mode (peak) diameter was ~20 nm at lower temperatures and increased at ~500 °C (~40 min) when Kapton became thermally unstable. The maximum mode diameter (~100 nm) and mass concentration were observed shortly after the temperature reached 640 °C (46 min). The particle number concentration remained high until the heater was turned off.

The number-based particle size distribution (PSD) snapshots at four instances during Kapton heating show lognormal distributions (Fig. 2c). At 46 min, the geometric mean diameter (d_g) was 93 nm, and the geometric standard deviation (σ_g) was 1.88. The WSSG has not been used in low gravity experiments; however, the Smoke Aerosol Measurement Experiment (SAME) was performed on ISS twice and the equipment was returned to Earth to repeat the smoke experiments [14,15,41]. Meyer et al. [14] reported that fresh particles from overheating of Kapton at 510 °C under normal gravity had a lognormal distribution with a d_g of 139 nm and σ_g of 1.78; at 557 °C, the d_g and σ_g were 140 nm and 1.63, respectively. These particles were slightly larger than those measured in this study, probably because they used a direct heating method with a coil of heater wire wrapped around the sample. Additionally, they used a 208 L drum to stabilize particle concentrations before measurement by the scanning mobility particle sizer (SMPS), which could cause more losses of smaller particles by diffusion and increase particle size due to coagulation.

Other SAME publications reported PSDs from transmission electron microscopy (TEM) of particles collected with a thermal precipitator on ISS [15,41]. They demonstrated that in the absence of buoyant flow under microgravity conditions, particles might grow larger due to coagulation and condensation as products from thermal decomposition concentrated near the flame [41] or overheating fuel [15]. Comparison of SAME ISS and ground test results show that under the same atmospheric pressure, oxygen level, and convective flow conditions, the PSDs were similar between microgravity and Earth gravity. However, microgravity experiments with no convective flow showed much larger particle sizes (about a factor of two) as compared to normal flow conditions (8 cm/s) in the ISS [15]. Particle morphology also changed from no flow (individual spheres) to ISS flow (partially fused clusters) for Pyrell smoke. The SAME experiment provided a unique opportunity to

explore the effects of microgravity on smoke particle formation; however, the no-flow test conditions are not relevant for crewed cabin environments, where requirements dictate a well-mixed cabin to eliminate CO_2 pockets. These studies demonstrate that environmental conditions such as gravity, convective flow rate, heating temperature, ambient pressure, and oxygen concentration significantly influence smoke particle sizes and concentrations. Additionally, different heating methods and fuel preparation (sizes and surface area of samples) affect smoke characteristics, making direct comparison of results from different studies difficult.

3.1.2. PTFE

The most striking observation from PTFE tests was that silica-containing surfaces in direct contact with PTFE were damaged during heating. Fig. 3a shows that the mica sheet before PTFE testing had no signs of degradation except for some defects from the previous heating experiment. After three tests, Fig. 3b shows that not only did the mica surface color change from gray to a pinkish hue, but the mica sheet's structural integrity was also lost. The mica became much thinner, weaker, and more brittle than in its original form. This change indicates a fluorination reaction between mica (a group of silicate minerals) and HF, resulting in the formation of silicon tetrafluoride (SiF_4) and water. The reaction can be simplified as:

$$SiO_2 + 4HF \rightarrow SiF_4 + 2H_2O \quad (2)$$

SiF_4 emissions from PTFE thermal decomposition in quartz reactors have been previously reported [42]. Further evidence of this reaction is shown in Fig. 3c, where a PTFE sample was heated in a porcelain crucible, causing the crucible surface to be etched and create hydrophobic spots. This reaction mechanism, along with potential losses on walls, may lead to underestimates of the EF of HF.

A range of fluoride gases were observed in PTFE tests. As shown in Fig. 4a, carbonyl fluoride (COF_2), octafluorocyclobutane (C_4F_8; also known as Freon-C-318), hexafluoropropylene (C_3F_6), and tetrafluoroethylene (C_2F_4) consistently started emitting around 550 °C then stopping within 6 min after the maximum temperature (640 °C) was reached. Similar emissions have been previously observed in PTFE pyrolysis [43]. COF_2 is more toxic than HF: a 10-min exposure at 0.35 ppm can be disabling and at 10 ppm can be lethal [44]. C_2F_4 is the unpolymerized form of PTFE [45]. Fig. S7 shows that the measured HF concentration was low, although peaks of gaseous SiF_4 were observed due to the fluorination reaction (Eq. (2)).

Fig. 4b and Fig. S8 show that particle number concentrations started to increase with temperatures exceeding ~250 °C (20 min) with a local maximum at ~350 °C (~25 min). The particle concentrations and mode diameters rapidly rose after ~510 °C (~35 min) with maxima at ~45 min. The multiple peaks in particle number concentration in Fig. 4b indicate several stages of PTFE decomposition. Although the particle number concentrations were similar between PTFE (Fig. 4b) and Kapton

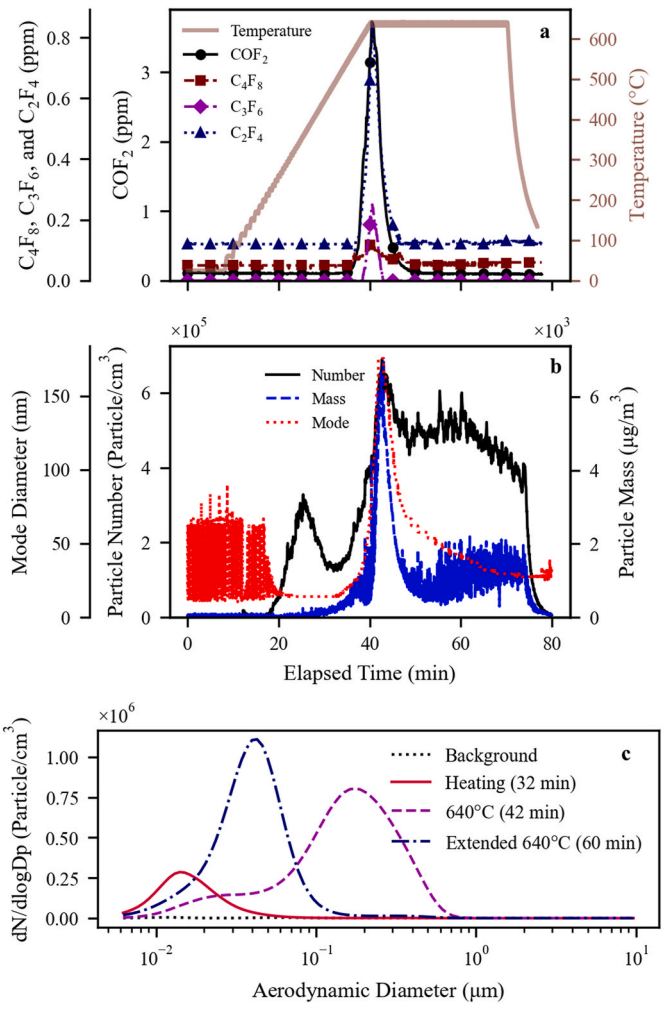

Fig. 4. Results from a PTFE experiment: a) time series of gas concentrations with temperature for carbonyl fluoride (COF_2), octafluorocyclobutane (C_4F_8), hexafluoropropylene (C_3F_6), and tetrafluoroethylene (C_2F_4); b) time series of particle number and mass concentrations as well as mode diameter; c) snapshots of particle size distributions at four stages: background, during the heat ramping, when the max setpoint was reached, and the extended heating at 640 °C.

(Fig. 2b), the mass concentrations from the PTFE tests were about an order of magnitude higher than those in the Kapton tests due to Kapton's higher thermal stability. PTFE emissions had a larger maximum mode diameter (180 nm) than Kapton (100 nm).

Fig. 4c and Fig. S8 show that submicron particles had bimodal

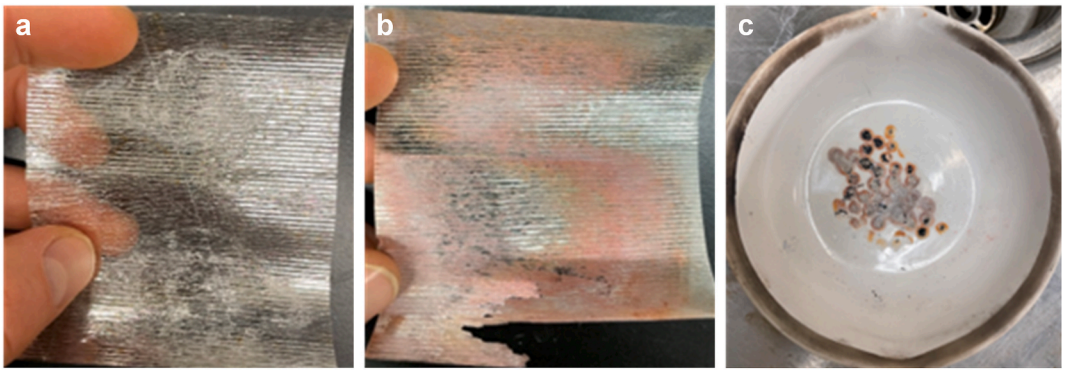

Fig. 3. Photographs of: a) mica sheet before PTFE tests; b) mica sheet after three PTFE tests; and c) crucible after heating PTFE samples.

distributions, with a smaller mode centered around 10–50 nm and a larger mode centered around 200–500 nm. The relative magnitudes of these two modes changed over the heating and temperature-soaking durations. In ground-based studies, PTFE pyrolysis generates polymer fragments that grow through nucleation and condensation to form ultrafine spherical particles, on the scale of 30 nm, corresponding to the smaller mode observed in these tests. These spherules collide and agglomerate leading to the fractal clusters corresponding to the larger mode [14,15,46,47].

Meyer et al. [14] reported that fresh particles from overheating of Teflon at 501 °C and normal gravity had a lognormal distribution with a d_g of 140 nm and σ_g of 2.22, which are similar to the distribution between 35 and 43 min in this study. At 512 °C, Meyer et al. [14] reported much larger sizes, with the d_g and σ_g being 250 nm and 2.07, respectively. These particles were larger than those with a maximum mode diameter of 180 nm measured at 640 °C in this study. The size distributions are sensitive to heating, dilution, and aging conditions.

3.1.3. TKT wire insulation

TKT wire insulation exhibited emissions similar to those of PTFE. As shown in Fig. 5, fluoride-based gases were emitted for all TKT tests. Similar to PTFE tests in Fig. 4a, the COF_2 concentrations from some TKT samples exceeded the Acute Exposure Guideline Level 3 of 1.0 ppm, which if exceeded for 10 min can be fatal [44]. NASA does not classify COF_2 in the SMACs guidelines for exposure limits. HCN and benzene were observed in TKT pyrolysis, but the concentrations were much lower than the Kapton tests. Fig. S9 shows that traces of SiF_4 were observed, likely formed from a fluorination reaction (Eq. (2)). Higher concentrations of HF were measured from TKT tests than from PTFE tests, possibly a result of reduced surface area contacting the mica sheet reducing the fluorination reaction.

The peak particle number concentrations from the TKT test (Fig. 5b) were about twice those of PTFE tests (Fig. 4b). The maximum mode diameter was 125 nm, between those for Kapton (100 nm) and PTFE (180 nm). Similar to the PTFE tests, a bimodal distribution was measured when the heater first reached 640 °C (Fig. 5c and Fig. S10). Because the TKT wire insulation is made of Kapton and PTFE, the particle properties resemble these two materials. Emissions of TKT were closer to PTFE than Kapton due to higher particle mass emissions from PTFE. It is also expected that the smoke detector responses will be similar to PTFE smoke particles.

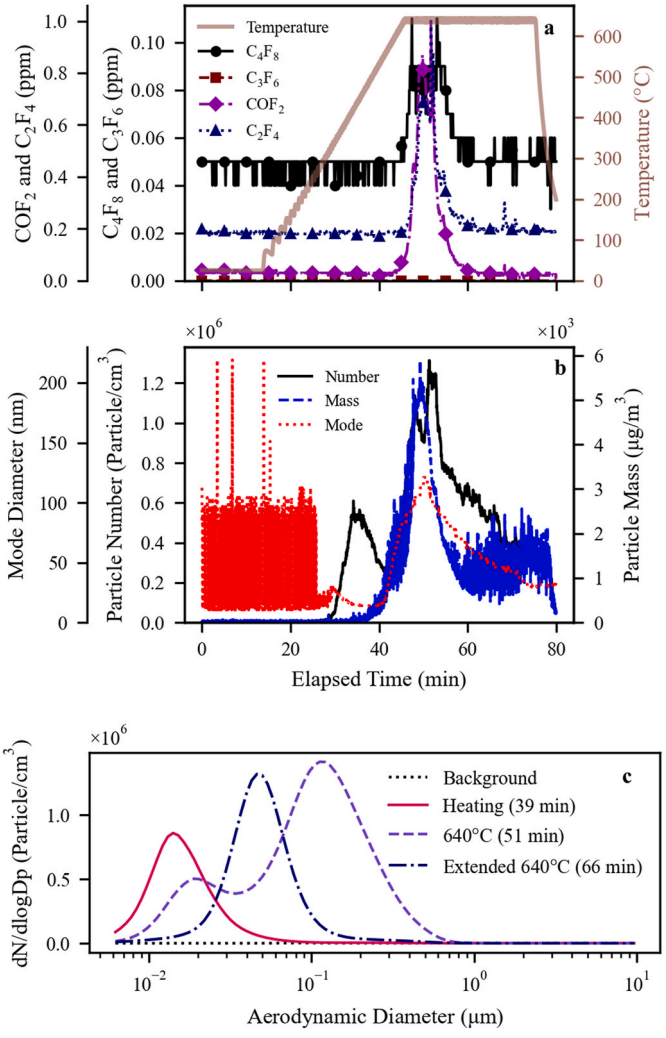

Fig. 5. Results from a TKT experiment: a) time series of gas concentrations with temperature for octafluorocyclobutane (C_4F_8), hexafluoropropylene (C_3F_6), carbonyl fluoride (COF_2), and tetrafluoroethylene (C_2F_4); b) time series of particle number and mass concentrations as well as mode diameter; c) snapshots of particle size distributions at four stages: background, during the heat ramping, when the max setpoint was reached, and the extended heating at 640 °C.

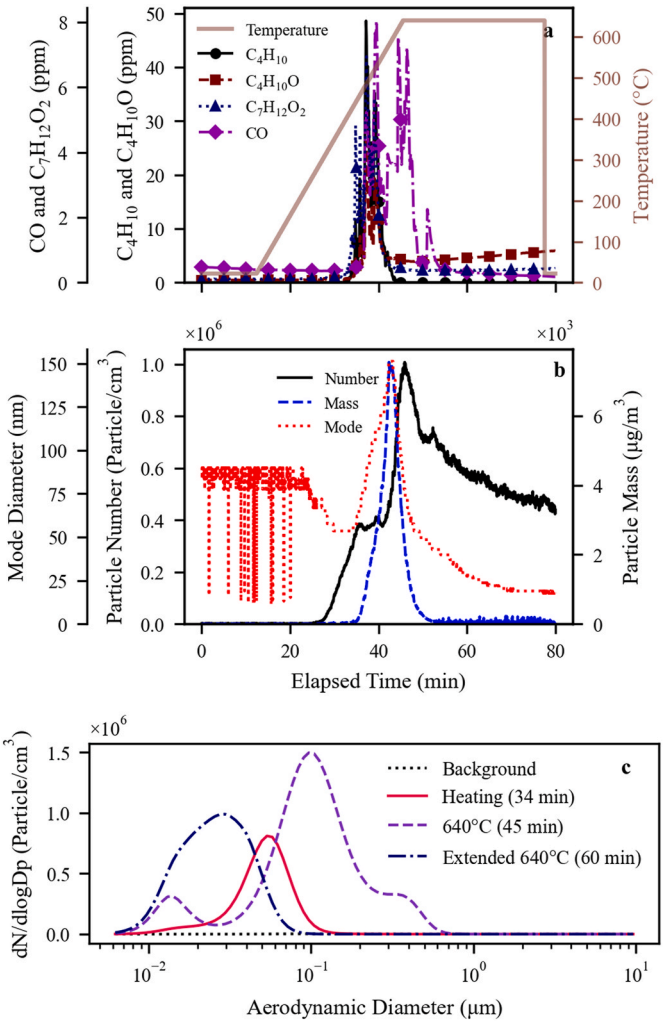

Fig. 6. Results from a Velcro™ experiment: a) time series of gas concentrations with temperature for butane (C_4H_{10}), 1-butanol ($C_4H_{10}O$), butyl acrylate ($C_7H_{12}O_2$), and carbon monoxide (CO); b) time series of particle number and mass concentrations as well as mode diameter; c) snapshots of particle size distributions at four stages: background, during the heat ramping, when the max setpoint was reached, and the extended heating at 640 °C.

3.1.4. Velcro™

Fig. 6a shows that Velcro™ had emissions of butane (C_4H_{10}), 1-butanol ($C_4H_{10}O$), and butyl acrylate ($C_7H_{12}O_2$), starting at ~400 °C and peaking at ~450–500 °C, indicating lower decomposition temperatures. These gases are mild irritants at the levels observed, with the primary concern being flammability for much higher concentrations, ~1000x the concentrations observed. NASA SMACs lists butanol gases as having impacts on both the eyes (irritation) and central nervous system (depression) for exposure of greater than 50 ppm for 1 h [38].

Temporal patterns of Velcro™ particle concentration in Fig. 6b are similar to those of PTFE in Fig. 4b. The mode diameter (~55 nm) was larger than for the other materials (~20 nm) earlier in the temperature ramping. The maximum mode diameter over the span of one test was 150 nm, between those for Kapton (100 nm) and PTFE (180 nm). When the temperature reached 640 °C, the size distributions were bimodal or trimodal (Fig. 6c and Fig. S11), probably related to different thermal decomposition behaviors of various materials in Velcro™.

3.1.5. Summary of emission characteristics

A variety of gaseous emissions were observed. Kapton and TKT emitted benzene, likely from Kapton as PTFE did not emit benzene. They also emitted HCN at potentially dangerous levels, even for small sample masses, relative to the room size. PTFE and TKT emitted substantial amounts of fluoride-based gases, consistent with PTFE's chemical composition. It is suspected that most HF emitted by the PTFE quickly reacted with the mica sheet and quartz tube to form SiF_4. Assuming no silicon were present, a larger amount of HF may have been observed for PTFE and TKT. As observed by Meyer et al. [12], HF can be difficult to quantify as it tends to stick to surfaces of all types. The levels of COF_2 emitted by both PTFE and TKT could be potentially fatal if exposure exceeds 10 min. Unique emissions from Velcro™ (i.e. butane, 1-butanol, and butyl acrylate) are not acutely toxic but potentially irritating [38] and may become flammable and/or explosive, characteristics which could exacerbate a developing spacecraft fire. The four materials emitted similar CO_2 levels despite having varying amounts of carbon by mass. This is likely due to the inefficient pyrolysis. Kapton was the only material generating significant (above 10 ppm) CO emissions. As previously mentioned, O_2 concentrations in Reno, NV are 17 % lower than sea level, which would influence combustion efficiency and CO emissions.

The time series of particle concentrations show similar patterns among the four materials with three phases: 1) when the heater reached 200–350 °C, particle number concentrations started to increase with the particle mode diameter $\lesssim$ 50 nm while mass concentrations remained close to background levels; 2) when the heater reached 550–640 °C, the particle mode diameter and mass concentration rapidly increased, with maxima observed around when the heater reached 640 °C; the number concentration reached maximum as well except for Kapton; and 3) during the extended heating at 640 °C, the mode diameter and mass concentrations gradually decreased; the number also decrease with the exception of Kapton. Most particle numbers were dominated by sizes <1000 nm, with mode diameter <200 nm for all materials. The submicron size range has bimodal or trimodal distributions, especially as temperatures reached 640 °C, although one of the modes typically dominates the number distributions.

Fig. 7 compares the size distributions of the four materials when the maximum temperature setpoint (640 °C) was reached. At this temperature, TKT emitted the smallest particles (mode at ~50 nm), followed by PTFE (mode at ~60 nm), Kapton (mode at ~75 nm), and Velcro™ (mode at ~100 nm). The smaller PTFE particles are consistent with the finding by Wang et al. [40], where Teflon particles generated the lowest sensitivity for a light-scattering smoke detector, but the highest sensitivity for an ionization smoke detector among several materials tested.

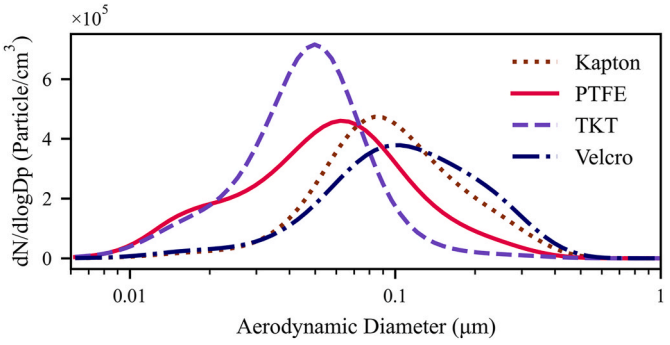

Fig. 7. Comparison of particle size distributions at 640 °C, the maximum temperature set point, for all four test materials: Kapton (brown dotted line), PTFE (red solid line), TKT (purple dashed line), and Velcro™ (blue dot-dashed line). (For interpretation of the references to color in this figure legend, the reader is referred to the Web version of this article.)

3.2. Particle charge distributions and chemical compositions

Fig. S12 shows an example of particle charge measurement for ELPI impactor stages 1–8 (corresponding to the particle size range of 6–314 nm) in a PTFE test. An electric current peak was observed overlapping the main particle number concentration peak around the maximum setpoint temperature. The current level and sign vary with the stage. Larger particle stages had low signal-to-noise ratios due to low particle concentrations and were not plotted.

The PTFE particle net charge distribution is shown in Fig. 8 and the distributions for all materials are in Fig. S13. Low net charges were found for all tested materials, with the number of elemental charges per particle <0.15, indicating that particles were close to electrically neutral. Therefore, it is not expected that the natural charges carried by particles from pyrolysis will influence the charge detection by ionization smoke detectors. In an ionization detector, alpha particles from the radioactive source ionize the air passing through the detector, providing a constant flow of ions to two charged plates inside the detector measured as a current. If smoke particulate enters the detection area, it stops the flow of ions by capturing the charge, thus triggering an alarm. If the particulate is already carrying a charge, the flow of ions may not reduce, impacting the effectiveness of the alarm. For Kapton, PTFE, and TKT, ELPI stages 2–4 (13.6–33.6 nm) consistently measured negative current, while stages 5 and 6 (50.7–98 nm) measured positive current. In contrast, Velcro™ emissions showed a positive current for stages 2–4, a negative current for stages 5–7 (50.7–169 nm) with higher charge levels, and a positive current for stage 8 (314 nm).

Among the $PM_{2.5}$ chemical components (Fig. S14), organic matter

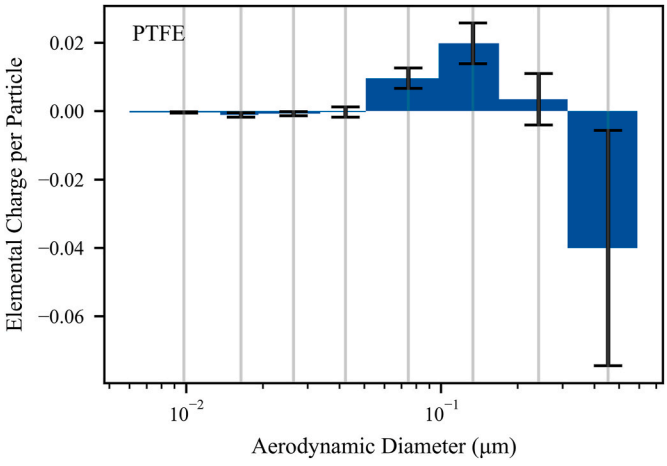

Fig. 8. Average net charge distribution of PTFE particles for ELPI stages 1–8. The error bars represent the standard error of the three tests.

(OM) is the largest contributor (>85 % of $PM_{2.5}$ mass) for all materials. Elemental carbon (EC) was present for Kapton (10 %), at a low level (0.1 %) for Velcro™, and below the detection limit for PTFE and TKT. PTFE (4.7 %) and TKT (3.4 %) had higher mineral abundances than Kapton and Velcro™ (<1 %), possibly due to the reaction of HF with the mica and quartz tube, which is supported by their higher abundance of particulate fluoride ions compared with Kapton and Velcro™. Because $PM_{2.5}$ can penetrate deep into the lung, detailed chemical composition information can help the assessment of the $PM_{2.5}$ health effects [48]. The detailed composition and toxicity of the organics warrant further research.

3.3. Emission factors (EFs)

Table 1 summarizes gas EFs for each material. The variabilities among replicate tests were high, as reflected by the large standard errors, compared to the means. The EFs for CO_2 were similar, ranging from 790 to 860 g/kg, likely because these experiments investigated thermal decomposition products from oxidative pyrolysis rather than combustion. These values are about half of the 1354–1780 g/kg EFs reported for smoldering cotton, Nomex, and Poly(methyl methacrylate) (PMMA) [16]. However, that study did not include the ash, CH_4, and VOC terms in Eq. (1). Wang et al. [35] found that excluding the ash or total carbon (TC) could cause EFs to be overestimated by a factor of six for pyrolysis. While the EFs from this study were lower than the smoldering combustion of damp vegetation (1124 g/kg) and food discards (955 ± 30 g/kg), they were higher than those for smoldering rubber (456 ± 41 g/kg) and plastic bottles (182 ± 30 g/kg) [35].

Kapton had the highest EFs for CO, about 10 times those for TKT and Velcro™, while PTFE had near-zero CO emissions. On the other hand, CH_4 EFs from Velcro™ were significantly higher than other materials. Kapton and TKT had unique emissions of benzene, while only PTFE and TKT had formaldehyde (CH_2O) emissions. As shown in Table S1, the nitrogen content was highest for Kapton (6.8 %) and Velcro™ (5.1 %). For Kapton, the high N resulted in very high EFs for HCN (192 ± 93 g/kg), but Velcro™ had a lower EF for HCN (4.8 ± 1.4 g/kg), and both Velcro™ and Kapton had high EFs for NH_3 (28–37 g/kg). Because TKT contains Kapton, it has detectable EFs for HCN (5.4 ± 2.4 g/kg) and NH_3 (0.58 ± 0.41 g/kg). Elevated EFs for butane, 1-butanol, and butyl acrylate (69–172 g/kg) were found in Velcro™.

Because PTFE contains a significant amount of fluorine as indicated by its molecular formula $(CF_2\text{-}CF_2)_n$, a range of fluoride-based gases were emitted from PTFE and TKT. PTFE had a low EF for HF (0.24 ± 0.12 g/kg), likely partly because HF had reacted with silicon-containing parts or stuck to surfaces before being measured by the FTIR (Fig. 3).

Table 2
Particulate emission factors (EFs) from pyrolysis of all test materials. The values are expressed as mean ± standard error from three repeated tests of each material. Unless otherwise specified, EFs are in g of species per kg of fuel (g/kg).

Species \EFs	Kapton	PTFE	TKT	Velcro™
$PM_{2.5}$ mass	2.78 ± 1.41	8.61 ± 4.33	29.42 ± 14.37	66.71 ± 27.03
OC	2.53 ± 0.27	2.85 ± 0.07	8.57 ± 0.34	60.89 ± 5.83
EC	0.35 ± 0.03	0 ± 0	0 ± 0	0.07 ± 0.13
$PM_{0.1}$ number (particles/kg)	3.99E+16 ± 6.51E+15	1.57E+16 ± 2.01E+14	7.39E+16 ± 1.96E+16	2.86E+16 ± 1.49E+16
PM_1 number (particles/kg)	4.22E+16 ± 7.46E+15	2.18E+16 ± 1.71E+15	1.01E+17 ± 3.47E+16	3.88E+16 ± 2.14E+16
$PM_{2.5}$ number (particles/kg)	4.22E+16 ± 7.46E+15	2.18E+16 ± 1.71E+15	1.01E+17 ± 3.47E+16	3.88E+16 ± 2.14E+16

Interestingly, TKT had much higher EFs for HF (26.2 ± 16.1 g/kg), suggesting that the combination of PTFE and Kapton may inhibit the loss of HF. The fluorination reaction product SiF_4 was detected (0.31–0.59 g/kg). TKT yielded higher EFs for other fluoride gases than PTFE.

Table 2 summarizes particulate EFs for each material. For $PM_{2.5}$ mass, Velcro™ had the highest EFs (66.7 ± 27.0 g/kg), followed by TKT (29.4 ± 14.4 g/kg). Wang et al. [16] reported $PM_{2.5}$ EFs in a similar range for smoldering materials, ranging from 166 ± 54 g/kg for PMMA, 90 ± 26 g/kg for Nomex, and 35.7 ± 4.6 g/kg for cotton. The $PM_{2.5}$ EFs for PTFE (8.6 ± 4.3 g/kg) and Kapton (2.8 ± 1.4 g/kg) were significantly lower than those for Velcro™ and TKT, and most smoldering materials from other studies [16,35]. EFs for flaming materials, i.e., PMMA (7.3 ± 0.7 g/kg) and cotton (8.4 ± 3.6 g/kg) were lower than their smoldering counterparts [16], showing that $PM_{2.5}$ EFs vary significantly with fuel materials and oxidation conditions.

OC constituted ~91 % of the $PM_{2.5}$ EFs for Kapton and Velcro™, and ~30 % for PTFE and TKT. EC for all materials accounted for minimal emissions with the highest EF of EC from Kapton at 0.35 g/kg. Fluorine compounds are expected to be abundant in $PM_{2.5}$ from PTFE and TKT emissions.

Particle number EFs (in particles/kg of fuel) were computed for $PM_{0.1}$, PM_1, and $PM_{2.5}$ fractions from the ELPI. As fewer particles were in the 1–2.5 μm size range, PM_1 and $PM_{2.5}$ were nearly identical. Ultrafine particles (i.e., $PM_{0.1}$) contributed >70 % of the total particle number: Kapton had the highest portion of $PM_{0.1}$ (95 %) followed by Velcro™ and TKT (both 73 %), and PTFE (72 %). TKT (1.07×10^{17} particles/kg) and PTFE (2.18×10^{16} particles/kg) had the highest and lowest $PM_{2.5}$ number EFs, respectively. These emission factors are plotted in Fig. S15

Table 1
Gaseous emission factors (EFs) from pyrolysis of all test materials. The values are expressed as mean ± standard error from three repeated tests of each material. EFs are in g of species per kg of fuel (g/kg).

Species \EFs	Kapton	PTFE	TKT	Velcro™
CO_2	859.85 ± 82.61	791.45 ± 8.90	847.52 ± 81.27	848.24 ± 119.21
CO	254.96 ± 80.57	0.02 ± 0.02	28.94 ± 8.71	22.79 ± 11.39
CH_4	10.14 ± 4.02	8.60 ± 5.40	2.11 ± 0.75	88.20 ± 57.46
NH_3	36.89 ± 21.70	–	0.58 ± 0.41	27.75 ± 10.46
Benzene	31.87 ± 9.95	–	3.48 ± 0.80	–
Formaldehyde	–	1.12 ± 0.38	3.14 ± 0.69	–
HCN	192.26 ± 92.87	0.61 ± 0.11	5.36 ± 2.35	4.76 ± 1.44
HF	0.20 ± 0.05	0.24 ± 0.12	26.15 ± 16.12	0.18 ± 0.05
Silicon tetrafluoride (SiF_4)	–	0.59 ± 0.29	0.31 ± 3.94	–
Octafluorocyclobutane (C_4F_8)	–	6.79 ± 2.89	10.49 ± 3.67	–
Hexafluoropropylene (C_3F_6)	–	3.04 ± 1.42	3.57 ± 21.77	–
Tetrafluoroethylene (C_2F_4)	–	11.06 ± 2.98	96.37 ± 58.10	–
Carbonyl Fluoride (COF_2)	–	38.85 ± 13.84	72.35 ± 49.02	–
Butane	–	–	–	124.56 ± 63.42
1-Butanol	–	–	–	171.87 ± 15.33
Butyl acrylate	–	–	–	68.84 ± 12.21

Note: CO_2 and CO were measured by Li-Cor 840A and Thermo 48i, respectively, while other gases were measured by the FTIR.

and are higher than those reported for biomass burning [49,50].

4. Conclusions

This study characterized gas and particle emissions from oxidative pyrolysis of four common spacecraft-relevant materials. Multiple gases that would cause immediate concern for the health of the astronauts were detected as per NIOSH guidelines and NASA SMACs. Multiple gases emitted are not classified within NASA SMACs guidelines. Kapton emitted HCN and CO at excessive concentrations. PTFE emitted multiple toxic fluorine-based gases that can pose immediate threats to life and equipment, especially COF_2 exceeded known safety guidelines. TKT shared emissions with both Kapton and PTFE with more contributions from PTFE than Kapton. Both TKT and PTFE emitted gases which resulted in a fluorination reaction with surfaces, which should be considered for surface corrosion protection and postfire clean-up procedures. Velcro™ emitted multiple flammable VOCs that could result in asphyxiation under high concentrations.

For all materials, a large number of submicron particles with bimodal or trimodal distributions were emitted. The mode diameter peaked in the 100–200 nm range for all materials as maximum temperature of 640 °C was reached. PTFE particles were smaller than those of other materials, consistent with a previous study showing that light scattering smoke detectors had the lowest sensitivity while ionization smoke detector had the highest sensitivity to PTFE smoke compared to other materials. The particles were nearly electrically neutral, carrying <0.15 net elementary charges per particle, indicating that the natural charge level would not affect ionization smoke detector sensitivity. Organics dominate the chemical composition of the emitted particulate, and their speciation and toxicity effects warrant further research.

Emission factors were quantified for the four materials for the first time. This data will be useful input for parameterizing smoke emissions in fire models [51,52].

CRediT authorship contribution statement

Bjoern Bingham: Writing – review & editing, Writing – original draft, Visualization, Validation, Software, Methodology, Investigation, Formal analysis, Data curation. **Salix Bair:** Investigation, Data curation. **Matthew Claassen:** Software, Investigation, Data curation. **Marit E. Meyer:** Writing – review & editing, Data curation, Conceptualization. **Claire Fortenberry:** Writing – review & editing, Methodology, Data curation, Conceptualization. **W. Patrick Arnott:** Writing – review & editing, Methodology, Investigation. **John G. Watson:** Writing – review & editing, Resources, Methodology, Conceptualization. **Judith C. Chow:** Writing – review & editing, Resources, Methodology. **Xiaoliang Wang:** Writing – review & editing, Writing – original draft, Visualization, Validation, Supervision, Resources, Project administration, Methodology, Investigation, Funding acquisition, Formal analysis, Data curation, Conceptualization.

Funding

This work was supported by the Nevada NASA Space Grant 80NSSC20M0043 22-24 and the Nevada NASA Space Grant Graduate Research Opportunity Fellowship.

Declaration of competing interest

The authors declare that they have no known competing financial interests or personal relationships that could have appeared to influence the work reported in this paper.

Acknowledgment

We thank Dr. Hans Moosmüller for the use of the combustion chamber where experiments were performed, Alita Regi for her assistance in the experiments and FTIR data processing, and Jim Cornish of Gasmet for his advice on FTIR analysis.

Appendix A. Supplementary data

Supplementary data to this article can be found online at https://doi.org/10.1016/j.firesaf.2025.104381.

Data availability

Data will be made available on request.

References

[1] NASA, Research Priorities for NASA Mission Directorates and Centers - Appendix H of National Space Grant College and Fellowship Program Opportunities in NASA STEM FY 2020-2024 Solicitation, National Aeronautics and Space Administration (NASA) Office of STEM Engagement, Washington, DC, 2019. https://www.nasa.gov/sites/default/files/atoms/files/sg_fy20-24_solicitiation_190916_archived-508.pdf.

[2] M.E. Meyer, D.L. Urban, G.W. Mulholland, V. Bryg, Z.-G. Yuan, G.A. Ruff, T. Cleary, J. Yang, Evaluation of spacecraft smoke detector performance in the low-gravity environment, Fire Saf. J. 98 (2018) 74–81, https://doi.org/10.1016/j.firesaf.2018.04.004.

[3] D. Dietrich, J. Niehaus, G. Ruff, D. Urban, F. Takahashi, J. Easton, A. Abbott, J. Graf, Determination of survivable fires, in: 42nd International Conference on Environmental Systems, 15-19 July 2012. San Diego, California.

[4] D.L. Urban, D.L. Dietrich, J.E. Booker, M.E. Meyer, G.A. Ruff, Fire detection tradeoffs as a function of vehicle parameters, in: 46th International Conference on Environmental Systems (ICES 2016), July 2016, pp. 10–14. Vienna, Austria.

[5] Stec, A.A. and Hull, T.R., *Fire Toxicity*. 2010, Cambridge, UK: Woodhead Publishing.

[6] B. Gardner, S. Denson, M. Huffman, T. Zimmerman, Recent major constituent analyzer performance on the international space station, in: 52nd International Conference on Environmental Systems, July 2023, pp. 16–20. Calgary, Canada.

[7] S. Madzunkov, C. Malone, J. Simcic, C. Jung-Kubiak, B. Bae, H. Kraus, D. Nikolić, V. Hristov, M. Homer, D. Fu, Progress report on the deployment of the second spacecraft atmosphere monitor technology demonstration instrument, in: 53rd International Conference on Environmental Systems, Louisville, Kentucky, 2024, pp. 21–25.

[8] M. Gisi, L. Pfeiffer, A. Stettner, E. Göhler, R. Seurig, B. Kraemer, A. Honne, K. Kaspersen, K. Bakke, A.E. Liverud, J. Thielemann, B. Elvesæter, P. Rebeyre, ANITA2 – multicomponent air analyser for ISS – 2 Years of operation, hardware behaviour and possible improvements for future versions, in: 53rd International Conference on Environmental Systems, Louisville, Kentucky, 21-25 July 2024.

[9] C. Fortenberry, M. Casteel, J. Graf, J. Easton, J. Niehaus, M. Meyer, D. Urban, G. Ruff, Evaluation of combustion products from large-scale spacecraft fires during the saffire-IV and saffire-V experiments, in: 50th International Conference on Environmental Systems, 12-14 July 2021.

[10] R.M. Briggs, M. Fradet, A. Ruff Gary, Results from the combustion product monitor on the saffire VI spacecraft fire safety experiment, in: 53rd International Conference on Environmental Systems, Louisville, Kentucky, 2024, pp. 21–25.

[11] P.D. Mudgett, M.R.C. Skow, T.F. Limero, S. Beck, J.S. Pilgrim, Seeking the tricorder: evolution of the NASA anomaly gas analyzer, in: 49th International Conference on Environmental Systems, 2019. Boston, Massachusetts.

[12] M.E. Meyer, P. Mudgett, S. Hornung, M. McClure, J.S. Pilgrim, V. Bryg, D. Makel, G.A. Ruff, G. Hunter, Materials combustion testing and combustion product sensor evaluations in FY12, in: 43rd International Conference on Environmental Systems, Vail, CO: American Institute of Aeronautics and Astronautics, 2013, https://doi.org/10.2514/6.2013-3432.

[13] C.E. Stockwell, R.J. Yokelson, S.M. Kreidenweis, A.L. Robinson, P.J. DeMott, R. C. Sullivan, J. Reardon, K.C. Ryan, D.W.T. Griffith, L. Stevens, Trace gas emissions from combustion of peat, crop residue, domestic biofuels, grasses, and other fuels: configuration and Fourier transform infrared (FTIR) component of the fourth Fire Lab at Missoula Experiment (FLAME-4), Atmos. Chem. Phys. 14 (18) (2014) 9727–9754, https://doi.org/10.5194/acp-14-9727-2014.

[14] M.E. Meyer, G.W. Mulholland, V. Bryg, D.L. Urban, Z.-G. Yuan, G.A. Ruff, T. Cleary, J. Yang, Smoke characterization and feasibility of the moment method for spacecraft fire detection, Aerosol. Sci. Technol. 49 (5) (2015) 299–309, https://doi.org/10.1080/02786826.2015.1025124.

[15] G.W. Mulholland, M. Meyer, D.L. Urban, G.A. Ruff, Z.-g. Yuan, V. Bryg, T. Cleary, J. Yang, Pyrolysis smoke generated under low-gravity conditions, Aerosol. Sci. Technol. 49 (5) (2015) 310–321, https://doi.org/10.1080/02786826.2015.1025125.

[16] X.L. Wang, H. Zhou, W.P. Arnott, M.E. Meyer, S. Taylor, H. Firouzkouhi, H. Moosmüller, J.C. Chow, J.G. Watson, Characterization of smoke for spacecraft fire safety, J. Aerosol Sci. 136 (2019) 36–47, https://doi.org/10.1016/j.jaerosci.2019.06.004.

[17] A. Järvinen, M. Aitomaa, A. Rostedt, J. Keskinen, J. Yli-Ojanperä, Calibration of the new electrical low pressure impactor (ELPI+), J. Aerosol Sci. 69 (2014) 150–159.

[18] S. Saari, A. Arffman, J. Harra, T. Rönkkö, J. Keskinen, Performance evaluation of the HR-ELPI+ inversion, Aerosol. Sci. Technol. 52 (9) (2018) 1037–1047.

[19] M. Marjamäki, J. Keskinen, D.-R. Chen, D.Y.H. Pui, Performance evaluation of the electrical low-pressure impactor (ELPI), J. Aerosol Sci. 31 (2) (2000) 249–261.

[20] J. Keskinen, K. Pietarinen, M. Lehtimäki, Electrical low pressure impactor, J. Aerosol Sci. 23 (4) (1992) 353–360, https://doi.org/10.1016/0021-8502(92)90004-F.

[21] W. Glover, H.-K. Chan, Electrostatic charge characterization of pharmaceutical aerosols using electrical low-pressure impaction (ELPI), J. Aerosol Sci. 35 (6) (2004) 755–764, https://doi.org/10.1016/j.jaerosci.2003.12.003.

[22] Dupont, DuPont™ Kapton®: summary of properties. https://www.dupont.com/content/dam/dupont/amer/us/en/ei-transformation/public/documents/en/EI-10142_Kapton-Summary-of-Properties.pdf, 2022. (Accessed 14 November 2023).

[23] G. Lopez, High-Performance polymers for aeronautic wires insulation: current uses and future prospects, Recent. Progress. Mater. 3 (1) (2021) 1–15, https://doi.org/10.21926/rpm.2101005.

[24] S.L. Olson, R.G. Sotos, *Combustion Of Velcro in Low Gravity*, NASA-TM-88970, NASA Lewis Research Center, Cleveland, OH, United States, 1987. https://ntrs.nasa.gov/archive/nasa/casi.ntrs.nasa.gov/19870010085.pdf.

[25] X.L. Wang, H. Zhou, W.P. Arnott, M.E. Meyer, S. Taylor, H. Firouzkouhi, H. Moosmüller, J.C. Chow, J.G. Watson, *Evaluation of Gas and particle Sensors for detecting spacecraft-relevant fire emissions* fire safety, Journal 113 (2020) 1–12, https://doi.org/10.1016/j.firesaf.2020.102977, 102977.

[26] M. Claassen, B. Bingham, J.C. Chow, J.G. Watson, Y. Wang, X.L. Wang, *Characterization of lithium-ion battery fire emissions—Part 1: chemical Composition of fine particles ($PM_{2.5}$)*, Batteries 10 (9) (2024) 301, https://doi.org/10.3390/batteries10090301.

[27] R. Krebs, J. Owens, H. Luckarift, Formation and detection of hydrogen fluoride gas during fire fighting scenarios, Fire Saf. J. 127 (2022) 103489, https://doi.org/10.1016/j.firesaf.2021.103489.

[28] M. Claassen, B. Bingham, J.C. Chow, J.G. Watson, Y. Wang, X.L. Wang, Characterization of lithium-ion battery fire emissions—Part 2: particle size distributions and emission factors, Batteries 10 (10) (2024) 366, https://doi.org/10.3390/batteries10100366.

[29] X.L. Wang, G. Chancellor, J. Evenstad, J.E. Farnsworth, A. Hase, G.M. Olson, A. Sreenath, J.K. Agarwal, A novel optical instrument for estimating size segregated aerosol mass concentration in real time, Aerosol. Sci. Technol. 43 (9) (2009) 939–950, https://doi.org/10.1080/02786820903045141.

[30] U. Pujala, S. Venkatesan, A. Kumar, S.P. Narayanam, V.S. Challa, V. Balasubramanian, Charging and dynamics of polystyrene latex aerosols under bipolar and unipolar ion field–ELPI measurements and comparison with charging theories, J. Electrost. 117 (2022) 103713, https://doi.org/10.1016/j.elstat.2022.103713.

[31] F.E. Ngohang, G. Fontaine, L. Gay, S. Bourbigot, Revisited investigation of fire behavior of ethylene vinyl acetate/aluminum trihydroxide using a combination of mass loss cone, Fourier transform infrared spectroscopy and electrical low pressure impactor, Polym. Degrad. Stabil. 106 (2014) 26–35, https://doi.org/10.1016/j.polymdegradstab.2014.01.019.

[32] X.L. Wang, H. Firouzkouhi, J.C. Chow, J.G. Watson, S.S.H. Ho, W. Carter, A.S. M. De Vos, Chemically speciated air pollutant emissions from open burning of household solid waste from South Africa, Atmos. Chem. Phys. 23 (24) (2023) 15375–15393, https://doi.org/10.5194/acp-23-15375-2023.

[33] L.-W.A. Chen, J.C. Chow, X.L. Wang, J.A. Robles, B. Sumlin, D.H. Lowenthal, R. Zimmermann, J.G. Watson, Multi-wavelength optical measurement to enhance thermal/optical analysis for carbonaceous aerosol, Atmos. Meas. Tech. 8 (2015) 451–461, https://doi.org/10.5194/amt-8-451-2015.

[34] J.C. Chow, D.H. Lowenthal, L.-W.A. Chen, X.L. Wang, J.G. Watson, *Mass reconstruction methods for $PM_{2.5}$: a review*, Air Qual. Atmos. Health 8 (3) (2015) 243–263, https://doi.org/10.1007/s11869-015-0338-3.

[35] X.L. Wang, H. Firouzkouhi, J.C. Chow, J.G. Watson, S.S.H. Ho, W. Carter, A.S. M. De Vos, Characterization of gas and particle emissions from open burning of household solid waste from South Africa, Atmos. Chem. Phys. 23 (2023) 8921–8937, https://doi.org/10.5194/acp-23-8921-2023.

[36] U.S. EPA, *Other Test Method 48 (OTM-48): Emission Factor Determination By the Carbon Balance Method* U.S. Environmental Protection Agency, U.S. EPA), Research Triangle Park, 2022. NC, https://www.epa.gov/system/files/documents/2022-08/Other%20Test%20Method%2048%20w%20Cover%20Letter.pdf.

[37] NIOSH, Immediately Dangerous to Life or Health (IDLH) Values, US Department of Health and Human Services, Centers for Disease Control and Prevention, 2019. National Institute for Occupational Safety and Health (NIOSH), https://www.cdc.gov/niosh/idlh/default.html.

[38] S. Langford, *Spacecraft Maximum Allowable Concentrations For Airborne Contaminants, Revision C* Lyndon B. Johnson Space Center, National Aeronautics and Space Administration (NASA), Houston, Texas, 2024. https://www.nasa.gov/wp-content/uploads/2024/06/jsc-20584-smacs-rev-c-final.pdf?emrc=17fbbc. (Accessed 26 November 2024).

[39] E.E. Ortelli, F. Geiger, T. Lippert, A. Wokaun, Pyrolysis of Kapton® in air: an in situ DRIFT study, Appl. Spectrosc. 55 (4) (2001) 412–419.

[40] X.L. Wang, J.C. Chow, J.G. Watson, M.E. Meyer, G.A. Ruff, J. Easton, G.M. Berger, P.D. Mudgett, Spacecraft smoke detector characterization with reference and smoke aerosols. 50th International Conference on Environmental Systems, 2020. https://ttu-ir.tdl.org/handle/2346/86366.

[41] D. Urban, G. Ruff, J. Brooker, T. Cleary, J. Yang, G. Mulholland, Z.-G. Yuan, Spacecraft fire detection: smoke properties and transport in low-gravity, in: 46th AIAA Aerospace Sciences Meeting and Exhibit, American Institute of Aeronautics and Astronautics, Reno, NV, 2008, https://doi.org/10.2514/6.2008-806.

[42] J.A. Conesa, R. Font, Polytetrafluoroethylene decomposition in air and nitrogen, Polym. Eng. Sci. 41 (12) (2001) 2137–2147, https://doi.org/10.1002/pen.10908.

[43] A.N. García, N. Viciano, R. Font, Products obtained in the fuel-rich combustion of PTFE at high temperature, J. Anal. Appl. Pyrolysis 80 (1) (2007) 85–91, https://doi.org/10.1016/j.jaap.2007.01.004.

[44] NASEM, Acute Exposure Guideline Levels For Selected Airborne Chemicals: Volume 18, The National Academies Press. National Academies of Sciences, Engineering, and Medicine (NASEM), Washington, DC, 2024, p. 179.

[45] G.J. Puts, P. Crouse, B.M. Ameduri, Polytetrafluoroethylene: synthesis and characterization of the original extreme polymer, Chem. Rev. 119 (3) (2019) 1763–1805, https://doi.org/10.1021/acs.chemrev.8b00458.

[46] W.C. Seidel, K.V. Scherer Jr., D. Cline Jr., A.H. Olson, J.K. Bonesteel, D.F. Church, S. Nuggehalli, W.A. Pryor, Chemical, physical, and toxicological characterization of fumes produced by heating tetrafluoroethene homopolymer and its copolymers with hexafluoropropene and perfluoro (propyl vinyl ether), Chem. Res. Toxicol. 4 (2) (1991) 229–236, https://doi.org/10.1021/tx00020a017.

[47] M.E. Meyer, *Particle Morphology And Elemental Composition Of Smoke Generated By Overheating Common Spacecraft Materials*, NASA/TM—2015-218891, NASA Glenn Research Center, Cleveland, Ohio, 2015. https://ntrs.nasa.gov/search.jsp?R=20160000940.

[48] P. Thangavel, D. Park, Y.C. Lee, Recent insights into particulate matter (PM(2.5))-mediated toxicity in humans: an overview, Int J Environ Res Public Health 19 (12) (2022), https://doi.org/10.3390/ijerph19127511.

[49] S. Janhäll, M.O. Andreae, U. Pöschl, Biomass burning aerosol emissions from vegetation fires: particle number and mass emission factors and size distributions, Atmos. Chem. Phys. 10 (3) (2010) 1427–1439, https://doi.org/10.5194/acp-10-1427-2010.

[50] A.Y.P. Wardoyo, L. Morawska, Z.D. Ristovski, J. Marsh, Quantification of particle number and mass emission factors from combustion of queensland trees, Environ. Sci. Technol. 40 (18) (2006) 5696–5703, https://doi.org/10.1021/es0609497.

[51] T.-K. Hong, S.-H. Park, Numerical analysis of smoke behavior and detection of solid combustible fire developed in manned exploration module based on exploration gravity, Fire 4 (4) (2021) 85.

[52] J. Brooker, D. Dietrich, S. Gokoglu, G. Ruff, D. Urban, A comparison of CFD and lumped capacity analyses of fires in spacecraft, in: 49th International Conference on Environmental Systems, 7 - 11 July 2019. Boston, Massachusetts.